2005

Development of the fast neutron imaging telescope

U Bravar
University of New Hampshire - Main Campus

P J. Bruillard
University of New Hampshire - Main Campus

E O. Fluckiger
Universität Bern

John R. Macri
University of New Hampshire - Main Campus, John.Macri@unh.edu

A L. MacKinnon
University of Glasgow

See next page for additional authors

Recommended Citation

Bravar, U.; Bruillard, P.J.; Fluckiger, E.O.; Macri, J.R.; MacKinnon, A.L.; McConnell, M.L.; Moser, M.R.; Ryan, J.M.; Woolf, R.S., "Development of the fast neutron imaging telescope," Nuclear Science Symposium Conference Record, 2005 IEEE , vol.1, no., pp.107,111, 23-29 Oct. 2005

Development of the Fast Neutron Imaging Telescope

Ulisse Bravar, Paul J. Bruillard, Erwin O. Flückiger, John R. Macri, Alec L. MacKinnon, Mark L. McConnell, Michael R. Moser, James M. Ryan, and Richard S. Woolf

***Abstract*–We report on the development of a next generation neutron telescope, with imaging and energy measurement capabilities, sensitive to neutrons in the 2-20 MeV energy range. The *Fast Neutron Imaging Telescope* (FNIT) was initially conceived to study solar neutrons as a candidate instrument for the Inner Heliosphere Sentinels (IHS) program under formulation at NASA. This detector is now being adapted to locate Special Nuclear Material (SNM) for homeland security purposes by detecting fission neutrons and reconstructing the image of their source. In either case, the detection principle is based on multiple elastic neutron-proton scatterings in organic scintillator. By reconstructing the scattering coordinates and measuring the recoil proton energy, the direction and energy of each neutron can be determined and discrete neutron sources identified. We describe the performance of the FNIT prototype, report on the current status of R&D efforts and present the results of recent laboratory measurements.**

I. Introduction

THIS paper describes a compact *Fast Neutron Imaging Telescope* (FNIT) for the measurement of neutrons in the 2-20 MeV energy range. The first full prototype of FNIT was recently assembled at the University of New Hampshire (UNH) and is presently undergoing performance testing.

The applications of FNIT are twofold. It was first conceived as a candidate detector for the Inner Heliosphere Sentinels (IHS) spacecraft program [1], presently in the formulation stage at NASA, to study neutrons from solar flares. In addition, its energy range and imaging capabilities make it also an ideal instrument for the identification of samples of Special Nuclear Material (SNM) through their neutron signature for homeland security purposes.

Manuscript received November 11, 2005. This work was supported in part by the U.S. Department of Energy under Contract DE-FG52-04NA25687 and NASA under grant NAG5-13519 in the United States and the Swiss National Science Foundation under grant 200020-105435/1 in Switzerland.

U. Bravar is with the Space Science Center, University of New Hampshire, Durham, NH 03824, USA (e-mail: ulisse.bravar@unh.edu).

P. J. Bruillard is with the Space Science Center, University of New Hampshire, Durham, NH 03824, USA (e-mail: pjb3@cisunix.unh.edu).

E. O. Flückiger is with the Physikalisches Institut, University of Bern, CH-3012 Bern, Switzerland (e-mail: erwin.flueckiger@phim.unibe.ch).

J. R. Macri is with the Space Science Center, University of New Hampshire, Durham, NH 03824, USA (e-mail: john.macri@unh.edu).

A. L. MacKinnon is with the Dept. of Physics and Astronomy, University of Glasgow, G12 8QQ, Scotland (e-mail: a.l.mackinnon@physics.gla.ac.uk).

M. L. McConnell is with the Space Science Center, University of New Hampshire, Durham, NH 03824, USA (e-mail: mark.mcconnell@unh.edu).

M. R. Moser is with the Physikalisches Institut, University of Bern, CH-3012 Bern, Switzerland (e-mail: michael.moser@phim.unibe.ch).

J. M. Ryan is with the Space Science Center, University of New Hampshire, Durham, NH 03824, USA (e-mail: james.ryan@unh.edu).

R. S. Woolf is with the Space Science Center, University of New Hampshire, Durham, NH 03824, USA (e-mail: rwoolf@cisunix.unh.edu).

II. Solar Neutrons

Neutrons in the MeV energy range produced in solar flares provide key information on the time evolution of the spectra of accelerated protons and ions at the flare site. They uniquely sample a wide range of the proton energy spectrum, and their numbers reflect the composition of the high-energy ions. When combined with γ-ray data, one has indicators and measures of the proton and ion spectra from a few MeV up to GeV energies [2].

With the proton spectrum determined at the low MeV end by way of γ-ray line ratios and at the high MeV end by way of π-related emission, one must question the need to measure anything else. Over the last two solar cycles we witnessed many solar flares not exhibiting γ-ray emission above 50 MeV and with insufficient energy for π-production. In such cases, the only way of determining the ion flux above ~40 MeV/nucleon is by measuring the neutron spectrum, which is continuous through the entire MeV range with no breaks [3].

FNIT was specifically designed by an international team for the 2-20 MeV energy range. A separate instrument, the *SOlar Neutron TRACking imaging spectrometer* (SONTRAC), was developed by the same team with the addition of University of Alabama – Huntsville, for higher energies (20-250 MeV) [4], [5]. Since low energy solar neutrons do not survive in significant numbers by the time they reach the Earth, energies below ~20 MeV are hardly accessible at 1 astronomical unit (AU). Therefore, customized neutron spectrometers have to be operated on missions to the innermost heliosphere.

The need to measure neutrons below 10 MeV has been recognized by NASA as one of the solar physics objectives. Considering the need to take measurements in close proximity to the Sun, the IHS program provides an ideal platform for the FNIT detector.

III. Special Nuclear Material

One of the critical gaps in homeland security is the inability to efficiently detect and identify kilogram-size samples of Special Nuclear Material (SNM). These materials, uranium and transuranics, emit neutrons via spontaneous or induced fission. Unlike other forms of radiation produced by SNM (e.g. γ-rays), copious and penetrating neutron emission is unique to fissionable material. Neutron detection, therefore, is of particular importance for SNM identification for security and proliferation deterrence.

Current detection systems often do not have sufficient sensitivity to detect problematic and dangerous amounts of fissionable material. For example, one kilogram of weapon grade plutonium (Pu) emits 6×10^4 neutrons/second. However,

this corresponds to little more than the background-level neutron flux at a distance of only several meters for a detector lacking imaging capability, as most present generation detectors do. As a consequence, the capability to search for clandestine amounts of SNM currently represents a major security shortcoming.

The energy spectrum of fission neutrons from Pu follows the Watt distribution, peaking at 1 MeV and with a mean value of ~2 MeV. In order to identify Pu samples, it is crucial to possess a detector with both imaging capability and an energy threshold of the order of 1 MeV. Both these requirements are satisfied by the FNIT design [6], [7].

IV. Neutron Detection and Imaging

Because they are electrically neutral, neutrons must be detected using indirect means. The preferred method at MeV energies takes advantage of the fact that the n-p elastic scattering cross section is large. The recoil proton from an n-p scatter is a highly ionizing particle and is easily detected with a suitable instrument. To employ this technique in its full potential, it is advantageous to have neutrons scatter off protons rather than heavier nuclei. Therefore, an ideal material, acting both as neutron scatterer and recoil proton detector, is organic scintillator [8].

To perform imaging, it is necessary for the neutron to undergo several (at least two) n-p scatters in the detector. One must be able to follow the path of the neutron, measuring the location, time and energy deposits of each n-p interaction.

Consider the case shown in Fig. 1. A neutron, whose incident direction is unknown, undergoes two n-p scatters. By measuring the coordinates and time difference of the two interactions, one can determine the energy and direction of the scattered neutron. By measuring the energy of the first recoil proton, one can then compute the energy of the incident neutron. The neutron scatter angle, θ_n, is given by:

$$\sin^2 \theta_n = \frac{E_{p1}}{E_n}$$

where E_{p1} and E_n are the energies of the first recoil proton and the incident neutron, respectively. Once E_{p1} and E_n are known, one can determine θ_n. In general, if the vector direction of the first recoil proton were known, one could determine the exact direction of the incident neutron. However, at FNIT energies, recoil proton tracks are too short for their orientation to be determined and one can only measure the proton's kinetic energy. With this information, knowing the direction of the recoil neutron, one can constrain the incident neutron's track to lie on the mantle of a cone.

By projecting the cone e.g. onto the celestial sphere, one can then define an "event circle" for each event, as shown in Fig. 1. Finally, from the intersection of several event circles, it is possible to obtain an image of the neutron source. The same principles are employed for γ-ray imaging in Compton telescopes. Namely, event circles from a source intersect at a specific point, while the imaging of an isotropic background produces circles with isotropically distributed intersections. This technique was demonstrated in the imaging of 20-80 MeV solar neutrons [9].

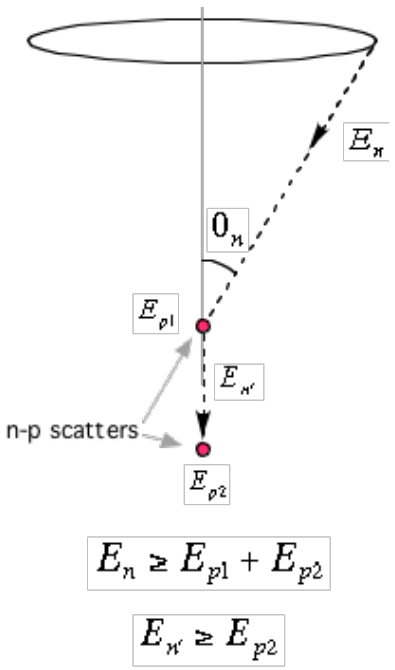

Fig. 1. Double elastic n-p scattering. The schematic displays the basic kinematics of event reconstruction. If the kinetic energy of the incident neutron is determined, the neutron arrival direction can be restricted to lie on the mantle of a cone. An "event circle", such as the one shown at the top of this figure, can then be drawn.

V. The Fast Neutron Imaging Telescope

The baseline design of FNIT in its full configuration is shown in Fig. 2. FNIT consists of a tower of eight to ten layers of position-sensitive plastic scintillator detectors operating in coincidence detection mode. For each elastic n-p scatter, the instrument measures the location, relative time and energy deposit of the recoil proton.

The scintillation light produced in each monolithic block of plastic scintillator is collected by a double-coordinate array of wavelength shifting (WLS) optic fibers and detected by a multianode photomultiplier tube (MAPMT). Its intensity is related to the kinetic energy of the scattered proton and position information can be extracted from the optic fiber mesh. Finally, the recoil neutron's time of flight (ToF) between layers is also measured and used to determine its momentum and for neutron / γ-ray discrimination. These data are analyzed on an event-by-event basis to determine each incident neutron's energy and event circle.

Figure 3 shows a picture of the full FNIT tower prototype consisting of three detector layers that was recently assembled at UNH and is presently undergoing performance testing. A coincidence between two or more layers is used for trigger. The design and setup of the individual detector layer is described in the following section.

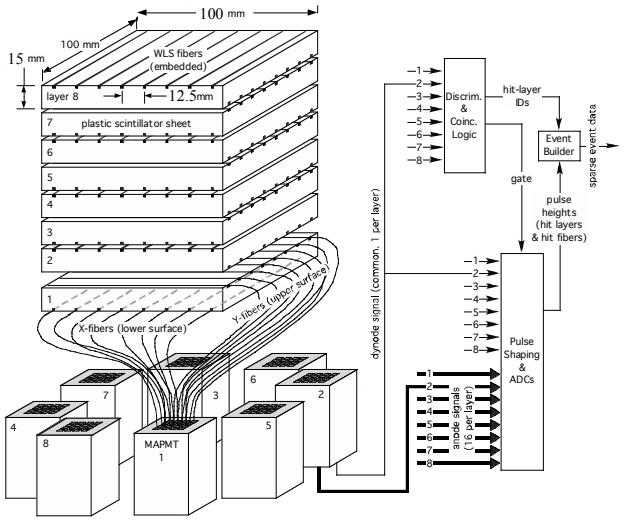

Fig. 2. Conceptual design of FNIT, including eight position sensitive plastic scintillator layers, WLS fibers coupled to MAPMTs and readout electronics. In this figure, each scintillator layer is 10×10 cm^2 in area, 1.5 cm thick and for clarity purposes is shown as incorporating only 16 WLS fibers. In the actual detector, each scintillator is 12×12 cm^2 in area and has 64 fibers.

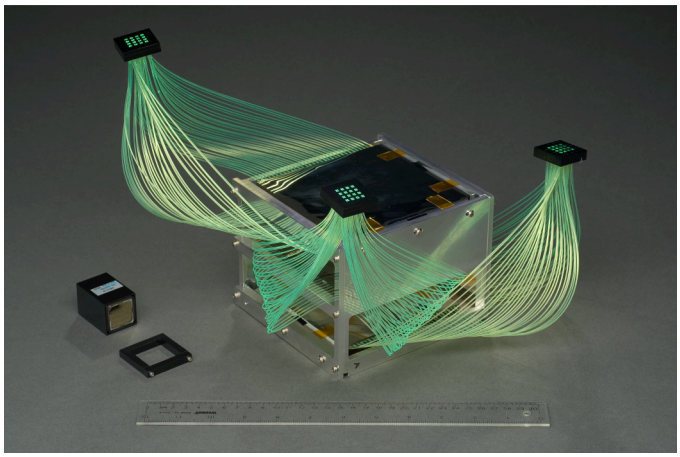

Fig. 3. Image of the full FNIT prototype. The aluminum structure hosts three 12×12 cm^2 scintillator layers placed on top of each other in a tower-like fashion. The surface area of the top scintillator, wrapped in reflective mylar, can be noticed at the center of the image. Three bundles of 64 green WLS fibers each are visible at the sides of the tower. They are grouped into three 4×4 arrays that are coupled to three MAPMTs, one of which is shown in the bottom left corner.

VI. Detector Layer Design

Each FNIT detector layer is made of a sheet of plastic scintillator. Grooves are machined into both surfaces of the sheet with a regular pitch and orthogonal orientations. A WLS fiber is bonded into each groove and routed to one pixel on the face of a MAPMT. A fraction of the blue scintillation light produced in the plastic scintillator is absorbed by the WLS fibers on both surfaces and re-emitted as green light. The clad WLS fibers act as light guides for the trapped portion of this green light signal that then travels the length of the fiber to the MAPMT pixel for readout. Maximizing the light yield is crucial to achieving the low energy threshold of the FNIT detector.

One 16-anode MAPMT measures the light from all the fibers of a single layer. When triggered, the IDs and pulse heights of the hit fibers are time-tagged and read out as event messages for further processing. Pulse height and ToF analysis are used to measure the energy deposits and interaction locations.

To determine the optimum structure of the detector layer, we manufactured several prototypes and conducted a number of key measurements, including light output and timing properties, plus spatial and energy resolution. We experimented with different scintillator plate dimensions, combined with various types of wrappings, fiber-extremity terminators and different fiber pitches, using both round and square WLS fibers. We also developed a Monte Carlo code based on the GEANT4 package [10] and used it in the optimization process and for design tradeoff studies.

Among the tested prototypes, the best performance was achieved by the following detector layer structure:

1. BC-404 plastic scintillator, 12 cm × 12 cm × 1.5 cm (thick) [11];
2. 64 evenly-spaced BCF-91A multi-clad WLS round fibers, diameter = 0.1 cm (32 x-fibers & 32 y-fibers) [11];
3. one Hamamatsu H8711-10, 16 channel MAPMT (4×4 array) [12];
4. 4-fiber groups read out by one MAPMT anode (i.e. 64 fibers feeding 16 MAPMT channels);
5. aluminized mylar wrapping of the large 12×12 cm^2 top and bottom surfaces of the scintillator layer;
6. polished aluminum end-mirrors to terminate the unused ends of the WLS fibers;
7. black coating to cover the edge surfaces of the plastic scintillator.

The bulk of the light signal from an n-p scattering is seen by two to four 4-fiber groups, as explained in the next section. The area of the detector layer is therefore fixed by the event rate and effective area that one wishes to achieve and the desired number of electronic readout channels rather than by single event detection performance requirements. On the other hand, the 1.5 cm scintillator thickness was chosen to have a ~10% probability of single n-p scatters per layer while minimizing the likelihood of double n-p scatters occurring in the same layer. The number / pitch of WLS fibers and the aluminized mylar wrapping were chosen to maximize light yield. Black coating of the side edges of the scintillator minimizes edge effects in the reconstruction of n-p scatter coordinates.

A photograph of the prototype scintillator layer described above is shown in Fig. 4. Note that the effective pitch of 4-fiber groups is approximately that of the thickness of the plate. Reasons for coupling a 4-fiber group to an individual MAPMT channel will become clear in the next section, when discussing position resolution.

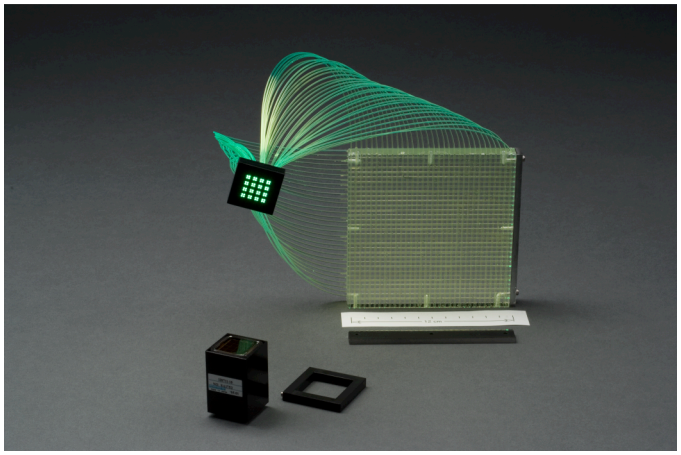

Fig. 4. FNIT prototype detector layer. The plastic scintillator, 12×12 cm^2 in area, is unwrapped. Two black terminators are visible next to the right and bottom scintillator edges. The 64 WLS fibers form an x-y mesh in the scintillator and are grouped into a 4×4 array of 16 pixels at one of the extremities. The 16-pixel element is coupled to the MAPMT shown in the foreground.

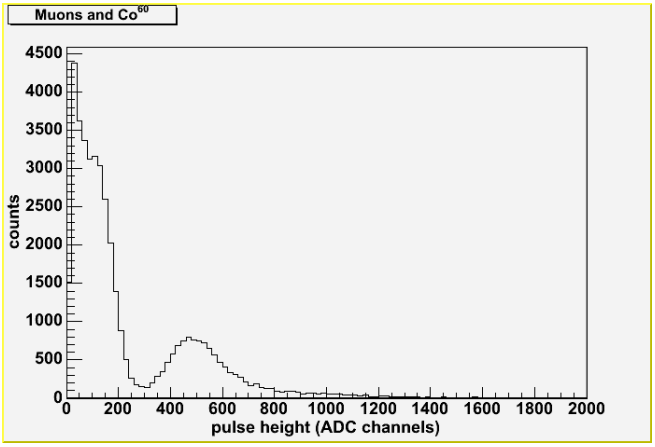

Fig. 5. ADC pulse height distribution in the FNIT prototype detector. The peak around ADC channel 500 is the cosmic-ray muon signal. The prototype was simultaneously irradiated with a ^{60}Co γ-ray source while acquiring these data. The Compton edge of our γ-source is the spectral feature around ADC channel 150.

VII. Detector Layer Performance

We evaluated the response of all of the prototype scintillator layers that we manufactured with standard laboratory β and γ radiation sources (^{241}Am, ^{57}Co, ^{133}Ba, ^{137}Cs, ^{60}Co, ^{90}Sr) and with cosmic-ray muons. Detector layers were augmented with a scintillator located on top of them that was used for coincidence trigger in μ-runs and ToF measurements. Data presented underneath are for the detector layer selected as being the one with the optimum structure that was described in the previous section.

We measured the light yield to be 41 photoelectrons / MeV (electron equivalent). Considering that a 1 MeV electron produces ~10^4 scintillation photons in our plastic scintillator, having determined with Monte Carlo simulations that ~2% of the initial number of photons (i.e. 200 photons) reach the photocathode, and taking into account a quantum efficiency of ~20%, the measured light yield is consistent with our expectations. Assuming a signal threshold of 10 photoelectrons, the corresponding energy threshold is 250 keV for electrons, which amounts to 1 MeV for protons [11]. Considering that two n-p recoil protons are needed for neutron imaging, the lower energy limit for neutrons is therefore ~2 MeV. It should be emphasized at this point that the stated high-energy limit of 20 MeV is not a hard threshold and the FNIT detector can in principle be used up to energies of a few hundred MeV. However, at higher energies, recoil proton *directions* can be determined with a tracking detector such as SONTRAC, providing a quality edge in neutron imaging over the event-circle technique employed by FNIT.

The energy resolution for the FNIT prototype was determined with cosmic-ray muons. The average ionization energy loss of a minimum ionizing muon in 1.5 cm of the BC-404 scintillator was calculated by our GEANT4 Monte Carlo code to be 2.5 MeV. The muon peak measured by the FNIT prototype detector is shown in Fig. 5. This distribution incorporates the fluctuations arising from three distinct effects:

1. Landau fluctuations in the ionization energy loss [13];
2. variable track length of cosmic-ray muons in the FNIT scintillator (due to their omni-directional flux);
3. fluctuations from detector noise and photon statistics.

Only the last of these three effects is representative of the energy resolution of the instrument. By deconvoluting the fluctuations caused by the first two effects, we determined the σ energy resolution for cosmic-ray muons to be $\delta E/E = 17\%$ at 2.5 MeV (electron equivalent). At this energy, ~100 photoelectrons are produced. Our δE/E figure is therefore comparable to the Poisson limit on the energy resolution due to photoelectron statistics (i.e. $\delta E/E \approx 10\%$).

Timing resolution was evaluated from ToF measurements between the FNIT prototype and the auxiliary scintillator located on top of it. From our setup we determined $\delta t = 0.6$ ns. To achieve good separation between Compton-scatter γ-rays and 10 MeV neutrons, we required the ToF of a 10 MeV neutron between adjacent FNIT layers in the full tower structure to be ~1 ns. Therefore, we fixed the vertical pitch of the FNIT tower at 4.5 cm, i.e. the gap between detector layers in the prototype shown in Fig. 3 was chosen to be 3 cm. Improving the δt figure is central to raising the quoted high-energy limit of the FNIT telescope.

Finally, position resolution was determined with a collimated ^{90}Sr β-source, at a β-electron energy of ~2 MeV, placed in the center of the prototype detector layer. The resulting distribution is shown in Fig. 6. The σ resolutions in the two horizontal axes are $\delta y = 0.45$ cm and $\delta x = 1.25$ cm. These figures are smaller than the vertical resolution $\delta z = 1.5$ cm, that arises from the scintillator thickness.

A legitimate question at this point is: why are δy and δx so different? The answer lies in the fact that the range of the ^{90}Sr β-electrons is shorter than the thickness of the FNIT

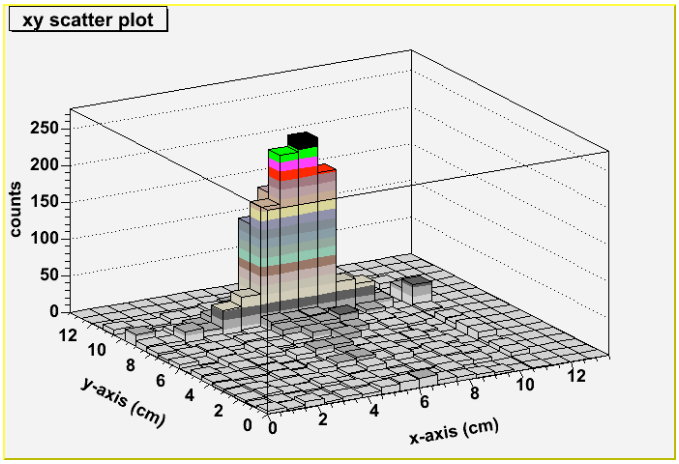

Fig. 6. Position resolution in the FNIT prototype detector. Reconstructed position in the x and y horizontal coordinates of a needle β-beam from a collimated ^{90}Sr source placed in the center of the FNIT detector layer. The differences in δx and δy are clearly visible.

scintillator layer and electrons undergo multiple scattering before stopping. Y-fibers are grooved into the top (irradiated) surface of the FNIT layer, while x-fibers are on its bottom surface. As a consequence, the light collected by the y-fibers is more localized than the light of the x-fibers. This effect places a limit on the position resolution one can achieve. Assuming that the typical n-p scatter occurs halfway through the thickness of the detector layer, and assuming conservatively that the multiple scattering limit applies to recoil protons as well, the average position resolution cannot get any better than approximately $(\delta x + \delta y) / 2 = 0.85$ cm.

It appears clear from Fig. 6 that in a 12×12 cm^2 detector layer, this resolution figure is achieved by a 16-channel MAPMT, reading out 4-fiber groups with a fiber-group pitch of 1.5 cm. While our tests showed that an increased number of WLS fibers (from 16 to 64) improves the light yield and therefore lowers the detector's energy threshold, replacing the 16-channel MAPMT with a 64-channel one would only increase the number of electronic readout channels without contributing to detector performance.

VIII. Conclusions

We provided a summary of the present status of the FNIT instrument. FNIT R&D efforts are at an advanced stage. Performance of the individual detector layer was fully evaluated and its design is now frozen. The first full tower prototype of FNIT has been assembled at UNH and performance testing is presently underway. Our next and final goal is to expose the FNIT prototype to a neutron source and demonstrate that this detector can in fact reconstruct the image of the source and measure its energy spectrum.

References

[1] http://lws.gsfc.nasa.gov/missions/sentinels/sentinels.htm
[2] J. A. Lockwood, H. Debrunner, and J. M. Ryan, "The Relationship Between Solar Flare Gamma-Ray Emission and Neutron Production," *Solar Phys*., vol. 173, pp.151-176, 1997.
[3] J. M. Ryan, "Long Duration Solar Gamma-Ray Flares," *Space Sci. Rev*., vol. 93, pp. 581-610, 2000.
[4] R. S. Miller, J. R. Macri, M. L. McConnell, J. M. Ryan, E. Flückiger, and L. Desorgher, "SONTRAC: An imaging spectrometer for MeV neutrons," *Nucl. Inst. Meth.*, vol. A505, pp. 36-40, 2003.
[5] U. Bravar, et al., "Atmospheric Neutron Measurements with the SONTRAC Science Model," these proceedings.
[6] N. Nereson, "Fission Neutron Spectrum of Pu^{239}," *Phys. Rev*., vol. 88, pp. 823-824, 1952.
[7] B. E. Watt, "Energy Spectrum of Neutrons from Thermal Fission of U^{235}," *Phys. Rev*., vol. 87, pp. 1037-1041, 1952.
[8] G. F. Knoll, *Radiation Detection and Measurement*, 3rd ed., New York: Wiley, 2000, pp. 553-563.
[9] H. Debrunner, et al., "Neutrons fron the 15 June 1991 Solar Flare," *Proc. 23rd Int. Cosmic Ray Conf*., vol. 3, pp. 115-118, 1993.
[10] S. Agostinelli, et al., "GEANT4: A Simulation Toolkit," *Nucl. Inst. Meth.*, vol. A506, pp. 250-303, 2003.
[11] http://www.photonic.saint-gobain.com
[12] http://www.hamamatsu.com
[13] L. D. Landau, *J. Exp. Phys. (USSR),* vol. 8, pp. 201-210, 1944.